Journal of Sound and Vibration 329 (2010) 5501–5519

Contents lists available at ScienceDirect

Journal of Sound and Vibration

journal homepage: www.elsevier.com/locate/jsvi

Mode localization phenomena and stability of disordered trains and train-like articulated systems travelling in confined fluid

Y. Sakuma *,[1], M.P. Païdoussis, S.J. Price

Department of Mechanical Engineering, McGill University, 817 Sherbrooke Street West, Montreal, Québec, Canada H3A 2K6

ARTICLE INFO

Article history:
Received 24 June 2009
Received in revised form
26 May 2010
Accepted 14 July 2010
Handling Editor: H. Ouyang
Available online 17 August 2010

ABSTRACT

The possible existence of mode localization in a chain of flexibly interconnected cylinders, representing a high-speed train travelling in a tunnel is investigated, in the presence of some disorder in the chain. Specifically, imperfections in the mass and springs in the model are considered as possible sources of mode localization, and it is shown that in general they can do so. This is part of a broader study into the dynamics of high-speed trains running in a tunnel, or more generally of a train-like system travelling in a coaxial cylindrical tube and subjected to aerodynamic forces associated with lateral motions of the cylinders. Each cylinder in the model is coupled to the other cylinders and is supported by springs, such that it has both translational and rotational degrees of freedom. Two models are used: a lumped-parameter Euler–Bernoulli beam model (LEB) and a lumped-parameter Timoshenko-beam model (LTB). The results of this study show that Timoshenko beam effects of rotational inertia and shear deformation have a considerable influence on the mode localization phenomena and that imperfections in the supporting springs have a considerable influence on the stability of the LTB model.

1. Introduction

Fluid–structure interactions of high-speed trains have been studied in Japan since 1986 as one of the issues affecting ride quality. As trains travel at higher speeds, the vibration amplitudes become greater, especially in tunnel sections. Vibrations and pressure fluctuations on the sides of the cars have been measured simultaneously, both in the open and in tunnel sections, and aerodynamic forces on the cars were calculated from the pressure data. It was found that lateral and yawing vibrations of the cars have a close correlation with the aerodynamic force acting on the cars [1–3]. To investigate the flow structure around the trains especially in tunnels, field measurements, wind tunnel experiments, and numerical simulations have been conducted [4–7]. Interested readers are encouraged to refer to [8] for more information.

Trains and train-like articulated systems consist of a chain of cars with similar mechanical properties, and consequently they can be considered as periodic structures (i.e. structures made up of a repeated basic substructure). Periodic structures generally possess some irregularities because the substructures cannot be produced precisely identical to each other; in addition, the structural properties change with age. Mode localization is the phenomenon of trapping vibrational energy in a specific part of a periodic structure when it has small structural irregularities (“disorder”). When mode localization occurs, the amplitude of a specific part of the structure is larger than for the rest. Thus, this phenomenon may cause serious

* Corresponding author. Tel.: +81 42 573 7318; fax: +81 42 573 7329.
E-mail address: sakuma@rtri.or.jp (Y. Sakuma).
[1] Present address: Railway Technical Research Institute, 2-8-38 Hikari-cho, Kokubunji-shi, Tokyo 185-8540, Japan.

0022-460X/$ - see front matter © 2010 Elsevier Ltd. All rights reserved.
doi:10.1016/j.jsv.2010.07.012

structural and/or dynamics problems. Consequently, investigation of the extent and sensitivity to mode localization is critical; moreover, the resultant changes to the mode shapes can be quite important.

Mode localization phenomena were first studied in the field of solid-state physics, in which the existence of localization of the electron eigenstates in a disordered solid was predicted [9]. Work in structural dynamics showed that vibrations in disordered periodic structures may be confined to a segment of the system due to structural irregularity; i.e., here too, mode localization phenomena may arise [10]. It was demonstrated theoretically and numerically that mode localization phenomena may occur in large space structures, where the importance of coupling strength between interconnected substructures was also investigated [11]. The structure is not sensitive to imperfections when the coupling between the substructures is strong. The phenomena of *weak* and *strong* localization were shown to occur for strong and weak coupling between substructures, respectively, in one-dimensional imperfect discrete [12] or continuous [13] structures. In Ref. [12] it was illustrated that weak localization occurs in systems with strong internal coupling and weak disorder while strong localization occurs in those with weak internal coupling and weak disorder. Strong vibration localization has been mainly studied in engineering structures because only a few substructures participate in the motion of the structure and they affect the dynamics of the structure considerably. Hence, here we mainly focus on strong localization and the word ''localization'' used in this paper means ''strong localization''.

A perturbation method was developed to obtain theoretically the localized modes of vibration of the disordered system of multi-span beams theoretically using Euler–Bernoulli beam theory [14]. Later, localization in multi-span beams on flexible supports was investigated using Timoshenko beam theory, which includes shear deformation and rotational inertia effects for dealing with higher-order modes [15]. Localization of oscillations in nonlinear systems has also been investigated [16,17] and a concept of nonlinear normal modes was proposed [18].

Most previous studies did not deal with systems of rigid bodies, but instead considered either *point masses* joined to each other by springs, or *continuous beams* on supports. In the present study, mode localization phenomena in a train of *rigid bodies* with elastic supports, joined to each other by translational and rotational springs and subjected to fluid dynamic forces are studied. The effect of imperfections in the mass, the supporting springs (either translational, or rotational) and the fluid dynamic forces on mode localization in finite-length train models are clarified by examining the mode shapes of the system.

In Section 2, the systems considered and the modelling assumptions are described [8,19]. Then the derivation of the equations of motion by the Lagrangian method is outlined; the equations are linearized, reduced to a standard eigenvalue problem, and solved numerically. In Section 3, the local and distributed imperfections considered in the analysis are described. In Section 4, mode localization phenomena in the LTB model *in still fluid* ($u=0$) are investigated by examining the mode shapes, and then the conditions of mode localization due to imperfections in the mass or springs are identified. In Section 5, mode localization phenomena in the LEB model *in still fluid* ($u=0$) are investigated. In Section 6, a discussion of mode localization in the LTB and LEB models is given. In Section 7, the dynamics of the disordered system of a LTB train *subjected to flow* is investigated. Finally, the conclusions are summarized in Section 8.

2. Theoretical model of the dynamics

The LTB and LEB models utilized in this paper have been developed in Refs. [19,8]. Accordingly, a highly abbreviated derivation of the equations of motion is given here.

2.1. Description of the system and assumptions

In order to achieve a description of the overall motion of a train passing through a tunnel, a large number of simplifying idealizations have to be introduced both in mechanics and fluid mechanics.

First, assumptions in mechanics are described. Simulation of translational and rotational motions of train dynamics commonly involves 17 or more degrees of freedom for each car and interaction between wheels and rails [20]. Since the main concern of the present study is to examine the effect of the aerodynamic forces on trains and train-like articulated systems, generally in the presence of some disorder, the simplest approach has been adopted: an actual vehicle with two bogies (wheel assemblies) is simplified to a cylindrical body supported only on two sets of translational springs and dampers; i.e., the bogies are modelled by springs and dampers. These cylindrical cars are coupled by springs and dampers and they can perform translational and rotational oscillatory motions in a cylindrical duct. It is assumed that there is no slip between the wheels and the rails in the lateral direction. In this situation, approximating the reaction of the rails against the lateral wheel motion by a spring-dashpot element is fully justified. It should be mentioned, however, that only the onset of train instability can be analyzed under this assumption.

The system under consideration is shown in Fig. 1. It consists of N rigid cylindrical cars that can only perform lateral translational $y^*(t)$ and yawing $\alpha(t)$ oscillatory motions of small amplitude in the cylindrical duct. Each car is attached to the duct (effectively the rails or the ''ground'') via two sets of translational springs and dampers (k_f, k_b, c_f, and c_b; f for front, b for back). Rotational and translational springs and dampers are also considered for interconnecting the cars (k_η, k_α, c_η, and c_α).

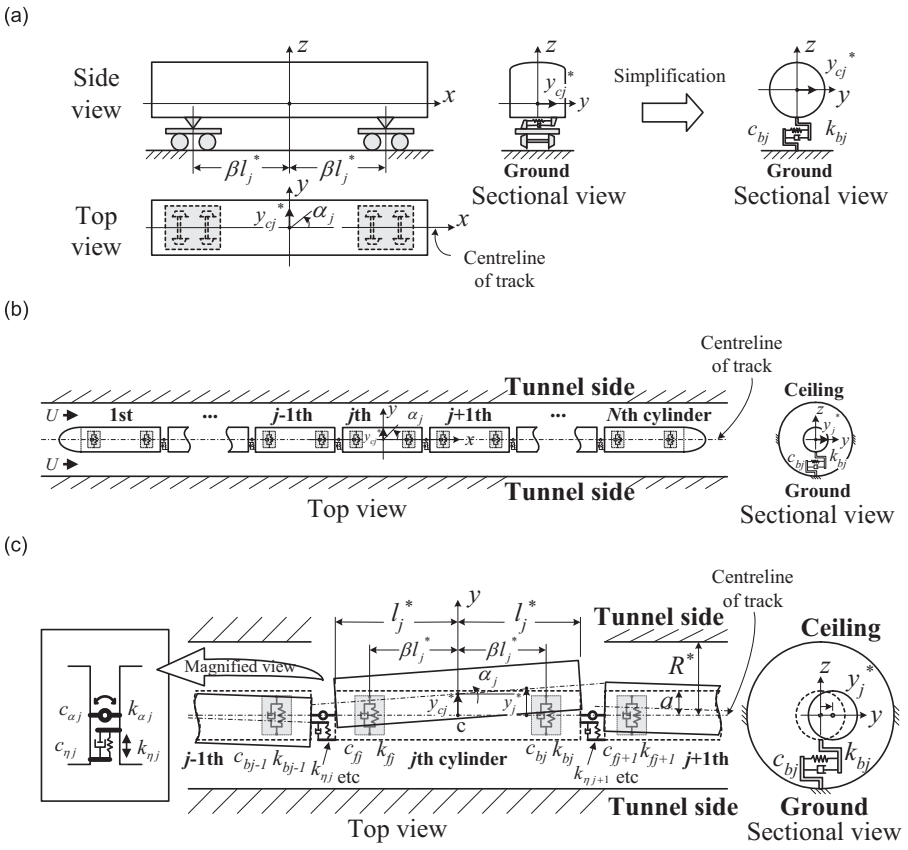

Fig. 1. Geometry of (a) a vehicle and a simplified cylindrical car, (b) N interconnected rigid cylindrical cars, and (c) the jth oscillating cylindrical car in the cylindrical duct. The variables with an asterisk are dimensional quantities.

The following assumptions in fluid mechanics are made: (a) the fluid is incompressible and of uniform density; (b) the leading and trailing cars comprise streamlined ends and no local separation of the flow takes place along the train; and (c) boundary layer development on the tunnel wall is ignored. Note that the pressure waves that exist in railway tunnels may be categorized into two main types: pressure waves generated when trains enter and leave tunnels, and those associated with boundary layer growth along the train [7,21–23]. The former change the speed of air flow as they travel back and forth in the tunnel but does not generate forced vibration of the train because the pressure waves can be considered as plane waves in the tunnel and thus aerodynamic forces acting on the two sides of the train cancel each other out. Representative of the latter type are the pressure fluctuations acting mainly on one of the two sides of the train, which results in forced vibration of the train. Since the effect of these pressure fluctuations on the dynamics has been studied in a previous study [8], they are not included here.

The forces associated with the structure itself are taken into account in the kinetic, dissipation and potential energies of the system. The fluid forces could in principle be determined by an appropriate solution of the Navier–Stokes equations. This will not be attempted here; instead, the fluid forces are determined essentially by superposition: inviscid and viscous forces are determined separately, based on Païdoussis's work [24,25]. This has been shown to be quite acceptable [24–26], even for more complex systems [26,27]. It has also been used for the train-like system considered here, in Refs. [19,8]. The hydrodynamic forces are incorporated partly in the kinetic energy and partly as generalized forces.

To obtain the equations of motion by application of the Lagrange equations, we now proceed to formulate the kinetic, dissipation, and potential energies of the system and the generalized forces.

2.2. Kinetic, dissipation, and potential energies of the structure

The kinetic energy of the jth car, T_{sj}, is

$$T_{sj} = \frac{1}{2} m_j \dot{y}_{cj}^*(t)^2 + \frac{1}{2} J_{cj} \dot{\alpha}_j(t)^2, \tag{1}$$

where m_j is the mass of the jth car and J_{cj} is its mass-moment of inertia about the centre of mass.

The dissipation energy of the jth car, D_{sj}, is

$$D_{sj}=\frac{1}{2}c_{fj}(\dot{y}^*_{cj}-\beta l^*_j\dot{\alpha}_j)^2+\frac{1}{2}c_{bj}(\dot{y}^*_{cj}+\beta l^*_j\dot{\alpha}_j)^2+\frac{1}{2}c_{\alpha j}(\dot{\alpha}_j-\dot{\alpha}_{j-1})^2+\frac{1}{2}c_{\eta j}\{(\dot{y}^*_{cj}-l^*_j\dot{\alpha}_j)-(\dot{y}^*_{cj-1}+l^*_{j-1}\dot{\alpha}_{j-1})\}^2$$
$$+\frac{1}{2}c_{\alpha j+1}(\dot{\alpha}_{j+1}-\dot{\alpha}_j)^2+\frac{1}{2}c_{\eta j+1}\{(\dot{y}^*_{cj+1}-l^*_{j+1}\dot{\alpha}_{j+1})-(\dot{y}^*_{cj}+l^*_j\dot{\alpha}_j)\}^2, \tag{2}$$

where β is the displacement coefficient for the supporting spring from the centre of the car as shown in Fig. 1(a) and l^*_j is the half-length of the jth car.

Finally, the potential energy of the jth car, V_{sj}, is

$$V_{sj}=\frac{1}{2}k_{fj}(y^*_{cj}-\beta l^*_j\alpha_j)^2+\frac{1}{2}k_{bj}(y^*_{cj}+\beta l^*_j\alpha_j)^2+\frac{1}{2}k_{\alpha j}(\alpha_j-\alpha_{j-1})^2+\frac{1}{2}k_{\eta j}\{(y^*_{cj}-l^*_j\alpha_j)-(y^*_{cj-1}+l^*_{j-1}\alpha_{j-1})\}^2$$
$$+\frac{1}{2}k_{\alpha j+1}(\alpha_{j+1}-\alpha_j)^2+\frac{1}{2}k_{\eta j+1}\{(y^*_{cj+1}-l^*_{j+1}\alpha_{j+1})-(y^*_{cj}+l^*_j\alpha_j)\}^2. \tag{3}$$

2.3. Kinetic energy of the fluid

The conservative inviscid part of the fluid dynamic forces can be included in the total kinetic energy of the system. Lighthill's [28] work, which is essentially an application of slender-body theory, is adopted. By this theory, the lateral velocity of the fluid on the inclined jth car moving laterally is given by (Fig. 2)

$$v_{fj}(\xi^*)=\dot{y}^*_j(t)=\dot{y}^*_{cj}(t)+\xi^*\dot{\alpha}_j(t)+U\alpha_j(t), \tag{4}$$

where U is the flow velocity in the space between the sides of the train and the tunnel in the train coordinate system; a detailed derivation may be found in Ref. [19]. The kinetic energy of the lateral fluid flow around the jth car is

$$T_{fj}=\int_{-l^*_j}^{l^*_j}\frac{1}{2}Mv^2_{fj}(\xi^*)\,\mathrm{d}\xi^*, \tag{5}$$

where $M=\chi\rho A$ is the virtual mass of the fluid for such lateral motions of the car, ρ is the fluid density, A is the cross-sectional area of the car, and $\chi=(R^{*2}+a^2)/(R^{*2}-a^2)$, where a is the radius of the cylindrical car and R^* the tunnel radius, is related to confinement by the tunnel. Substituting (4) into (5), one obtains

$$T_{fj}=\chi\rho Al^*_j\left\{\frac{1}{3}l^{*2}_j\dot{\alpha}_j(t)^2+(\dot{y}^*_{cj}(t)+U\alpha_j(t))^2\right\}. \tag{6}$$

2.4. The generalized forces on a middle (jth) car

Next, the nonconservative generalized forces will be derived. Forces other than the conservative inviscid fluid dynamic forces acting on the system are shown in Fig. 3: viscous forces, pressure gradient forces, nonconservative inviscid forces, and form drag. Apart from the leading (j=1) and trailing (j=N) cars, two aerodynamic forces (other than the inviscid ones) act on the middle cars (j=2,…,N): viscous and pressure gradient forces, as shown in Fig. 3.

The viscous forces per unit length of the jth car in the normal and longitudinal directions F_{Nj} and F_{Lj} are given by Taylor [29]:

$$F_{Nj}=\frac{1}{2}\rho D^*U^2(C_N\sin i+C_{Dp}\sin^2 i),\quad F_{Lj}=\frac{1}{2}\rho D^*U^2C_T\cos i, \tag{7}$$

where $i=\tan^{-1}(\partial y^*/\partial x^*)+\tan^{-1}\{(\partial y^*/\partial t)/U\}$ is the angle of inclination of the car to the flow, as in Fig. 4; D^* is the car diameter, C_N and C_T are the frictional drag coefficients in the normal and tangential directions, respectively, and C_{Dp} is the form drag coefficient. For small $\partial y^*/\partial x^*$ and $(\partial y^*/\partial t)/U$, Eq. (7) may be written as

$$F_{Nj}=\frac{1}{2}\rho D^*UC_N\left(\frac{\partial y^*_j}{\partial t}+U\frac{\partial y^*_j}{\partial x^*}\right)+\frac{1}{2}\rho D^*C_D\left(\frac{\partial y^*_j}{\partial t}\right),\quad F_{Lj}=\frac{1}{2}\rho D^*U^2C_T, \tag{8}$$

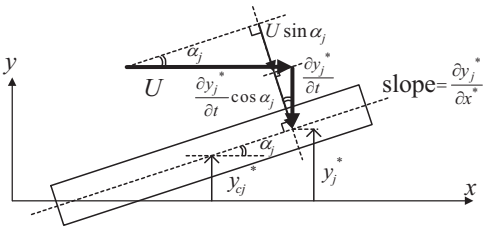

Fig. 2. Calculation of the relative fluid-body velocity in the normal direction of the jth cylindrical car.

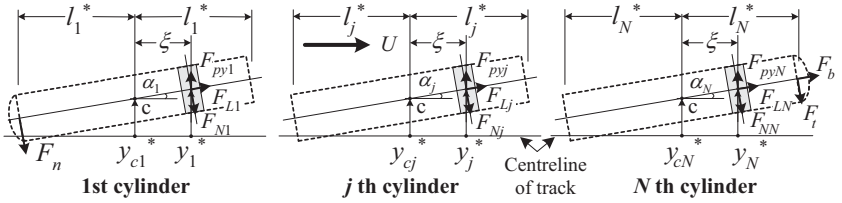

Fig. 3. Forces acting on cylindrical cars and on elements $d\xi$ of the 1st, jth, and N th cylindrical cars.

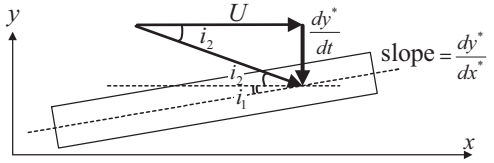

Fig. 4. Calculation of the angle of incidence i of the cylindrical car, $i=i_1+i_2$.

where the second term in F_N represents a linearization of the quadratic viscous force at zero flow velocity, $\frac{1}{2}\rho D^* C_{Dp}|\partial y_j^*/\partial t|(\partial y_j^*/\partial t)$, in which the drag coefficient represents $C_D = C_{Dp}|\partial y_j^*/\partial t|$.

The pressure gradient forces in the x and y directions acting on the jth car equipped with hoods are given by [19]

$$F_{px,j} = -2l_j^* A(1-\varepsilon)\frac{\mathrm{d}p}{\mathrm{d}x}, \quad F_{py,j} = -2l_j^* A(1-\varepsilon)\frac{\mathrm{d}p}{\mathrm{d}x}\alpha_j, \tag{9}$$

where ε is the ratio of cross-sectional area of the hood to that of the car. The pressure gradient distribution may be written as

$$A\frac{\mathrm{d}p}{\mathrm{d}x} = -\frac{1}{2}\rho D^* U^2 C_T\left(\frac{D^*}{D_h^*}\right) = -\frac{\rho a U^2 C_T}{r_h}, \tag{10}$$

where $D_h^*=2(R^*-a)$ is the hydraulic diameter and $r_h=(R^*-a)/a$ is the ratio of the gap to the car radius.

Therefore, the virtual work associated with the virtual displacement δW_j on the jth car is given by

$$\delta W_j = \int_{-l_j^*}^{l_j^*}(-F_{Nj}+F_{Lj}\alpha_j(t))\delta(y_{cj}^*(t)+\xi^*\alpha_j(t))\,\mathrm{d}\xi^* + \delta W_{pj}. \tag{11}$$

Substituting Eqs. (8)–(10) into (11), we obtain the generalized forces Q_{ycj} and $Q_{\alpha j}$ on the jth car, respectively, associated with translational and rotational motions; refer to [19].

2.5. Additional generalized forces on the leading and trailing cars

In addition to the forces already formulated for any typical "middle car," we take into account the nonconservative inviscid forces, F_n and F_t ("n" for nose, "t" for tail), and a form drag F_b acting on the leading ($j=1$) and trailing ($j=N$) cars, respectively, as shown in Fig. 3 [19].

The nonconservative inviscid forces acting on the nose and tail of the system, F_n and F_t, may be written as

$$F_n = -(1-f_n)\chi\rho AU\left(\frac{\partial y_1^*}{\partial t}+U\frac{\partial y_1^*}{\partial x^*}\right), \quad F_t = -(1-f_t)\chi\rho AU\left(\frac{\partial y_N^*}{\partial t}+U\frac{\partial y_N^*}{\partial x^*}\right), \tag{12}$$

where f_n and f_t are parameters that are equal to or less than unity, which take into account loss in lateral momentum flux due to the shape of the free end; for an ideally streamlined end, $f_n\to 1$ or $f_t\to 1$ [24,30]. The form drag of the trailing car, F_b, associated with separation of the flow is given by

$$F_b = \frac{1}{2}\rho D^{*2} U^2 C_b, \tag{13}$$

where C_b is the base drag coefficient.

The virtual work associated with the first and last cars will therefore have the additional terms

$$\delta W_1' = F_n\delta y_{c1}^*(t) - F_n l_1^*\delta\alpha_1(t), \tag{14}$$

$$\delta W_N' = \{F_t + F_b\alpha_N(t)\}\delta(y_{cN}^*(t)+l_N^*\alpha_N(t)), \tag{15}$$

respectively. Therefore, the appropriate additional generalized forces Q'_{yc1}, $Q'_{\alpha 1}$ and Q'_{ycN}, $Q'_{\alpha N}$ may be obtained [19].

2.6. The equations of motion

The total kinetic energy of the system, T, is given by $T=T_s+T_f$, where $T_s=\sum_{j=1}^{N} T_{sj}$ and $T_f=\sum_{j=1}^{N} T_{fj}$ are given by Eqs. (1) and (6), respectively. Similarly, $D=\sum_{j=1}^{N} D_{sj}$ and $V=\sum_{j=1}^{N} V_{sj}$. Eqs. (1)–(3), (6), and the generalized forces Q_{ycj} and $Q_{\alpha j}$, Q'_1 and $Q'_{\alpha 1}$, Q'_{ycN} and $Q'_{\alpha N}$, while taking the summation over j into account, are substituted into Lagrange's equations

$$\frac{\mathrm{d}}{\mathrm{d}t}\left(\frac{\partial T}{\partial \dot{q}_i}\right)-\frac{\partial T}{\partial q_i}+\frac{\partial D}{\partial \dot{q}_i}+\frac{\partial V}{\partial q_i}=Q_i,\quad q_1=y^*_{cj},\ q_2=\alpha_j,\ j=1,2,\ldots,N,$$

thereby obtaining the equations of motion. Introducing the dimensionless quantities

$$x=x^*/a,\quad y=y^*/a,\quad l=l^*/a,\quad D=D^*/a=2,\quad \tau=t\sqrt{\frac{k_0}{m_0 a}},\quad u=U\sqrt{\frac{m_0}{k_0 a}},$$

$$\omega=\Omega\sqrt{\frac{m_0 a}{k_0}},\quad \mu=\frac{M_0}{m_0},\quad \overline{k}_{\eta j}=\frac{k_{\eta j}}{k_0},\quad \overline{k}_{\alpha j}=\frac{k_{\alpha j}}{a^2 k_0},$$

$$\zeta_{\eta j}=\frac{c_{\eta j}}{\sqrt{k_0 m_0 a}},\quad \zeta_{\alpha j}=\frac{c_{\alpha j}}{a^2\sqrt{k_0 m_0 a}},\quad c=C_D\sqrt{\frac{m_0}{k_0 a}},$$

into the equations of motion, we obtain the dimensionless equations of motion for constant frictional viscous forces along the train:

$$\begin{aligned}
&2(1+\chi\mu)l_j\frac{\mathrm{d}^2 y_{cj}(\tau)}{\mathrm{d}\tau^2}+\delta_{j1}\chi\mu(1-f_n)u\frac{\mathrm{d}y_{c1}(\tau)}{\mathrm{d}\tau}-\zeta_{\eta j}\frac{\mathrm{d}y_{cj-1}(\tau)}{\mathrm{d}\tau}+\left\{\zeta_{fj}+\zeta_{bj}+\zeta_{\eta j}+\zeta_{\eta j+1}+\frac{2\mu l_j}{\pi}(uC_N+c)\right\}\frac{\mathrm{d}y_{cj}(\tau)}{\mathrm{d}\tau}-\zeta_{\eta j+1}\frac{\mathrm{d}y_{cj+1}(\tau)}{\mathrm{d}\tau}\\
&+\delta_{jN}\chi\mu(1-f_t)u\frac{\mathrm{d}y_{cN}(\tau)}{\mathrm{d}\tau}-\delta_{j1}\chi\mu(1-f_n)l_1 u\frac{\mathrm{d}\alpha_1(\tau)}{\mathrm{d}\tau}-\zeta_{\eta j}l_{j-1}\frac{\mathrm{d}\alpha_{j-1}(\tau)}{\mathrm{d}\tau}+\{-\beta\zeta_{fj}+\beta\zeta_{bj}-\zeta_{\eta j}+\zeta_{\eta j+1}+2\chi\mu u\}l_j\frac{\mathrm{d}\alpha_j(\tau)}{\mathrm{d}\tau}+\zeta_{\eta j+1}l_{j+1}\frac{\mathrm{d}\alpha_{j+1}(\tau)}{\mathrm{d}\tau}\\
&+\delta_{jN}\chi\mu(1-f_t)l_N u\frac{\mathrm{d}\alpha_N(\tau)}{\mathrm{d}\tau}-\overline{k}_{\eta j}y_{cj-1}(\tau)+(\overline{k}_{fj}+\overline{k}_{bj}+\overline{k}_{\eta j}+\overline{k}_{\eta j+1})y_{cj}(\tau)-\overline{k}_{\eta j+1}y_{cj+1}(\tau)+\delta_{j1}\chi\mu(1-f_n)u^2\alpha_1(\tau)-\overline{k}_{\eta j}l_{j-1}\alpha_{j-1}(\tau)\\
&+l_j\left[(-\beta\overline{k}_{fj}+\beta\overline{k}_{bj}-\overline{k}_{\eta j}+\overline{k}_{\eta j+1})-\frac{2\mu u^2}{\pi}\left\{\left(1-\frac{\varepsilon-1}{r_h}\right)C_T-C_N\right\}\right]\alpha_j(\tau)+\overline{k}_{\eta j+1}l_{j+1}\alpha_{j+1}(\tau)+\delta_{jN}\mu\left\{\chi(1-f_t)-\frac{2C_b}{\pi}\right\}u^2\alpha_N(\tau)=0,
\end{aligned}\tag{16}$$

$$\begin{aligned}
&2l_j\left\{\frac{1}{4}+\frac{l_j^2}{3}+\frac{1}{3}\chi\mu l_j^2\right\}\frac{\mathrm{d}^2\alpha_j(\tau)}{\mathrm{d}\tau^2}-\delta_{j1}\chi\mu(1-f_n)l_1 u\frac{\mathrm{d}y_{c1}(\tau)}{\mathrm{d}\tau}+\zeta_{\eta j}l_j\frac{\mathrm{d}y_{cj-1}(\tau)}{\mathrm{d}\tau}+\{(-\beta\zeta_{fj}+\beta\zeta_{bj}-\zeta_{\eta j}+\zeta_{\eta j+1})-2\chi\mu u\}l_j\frac{\mathrm{d}y_{cj}(\tau)}{\mathrm{d}\tau}-\zeta_{\eta j+1}l_j\frac{\mathrm{d}y_{cj+1}(\tau)}{\mathrm{d}\tau}\\
&+\delta_{jN}\chi\mu(1-f_t)l_N u\frac{\mathrm{d}y_{cN}(\tau)}{\mathrm{d}\tau}+\delta_{j1}\chi\mu(1-f_n)l_1^2 u\frac{\mathrm{d}\alpha_1(\tau)}{d\tau}+(-\zeta_{\alpha j}+\zeta_{\eta j}l_{j-1}l_j)\frac{\mathrm{d}\alpha_{j-1}(\tau)}{\mathrm{d}\tau}\\
&+\left\{(\beta^2\zeta_{fj}+\beta^2\zeta_{bj}+\zeta_{\eta j}+\zeta_{\eta j+1})l_j^2+\zeta_{\alpha j}+\zeta_{\alpha j+1}+\frac{2\mu l_j^3}{3\pi}(uC_N+c)\right\}\frac{\mathrm{d}\alpha_j(\tau)}{\mathrm{d}\tau}\\
&+(-\zeta_{\alpha j+1}+\zeta_{\eta j+1}l_j l_{j+1})\frac{\mathrm{d}\alpha_{j+1}(\tau)}{\mathrm{d}\tau}+\delta_{jN}\chi\mu(1-f_t)l_N^2 u\frac{\mathrm{d}\alpha_N(\tau)}{\mathrm{d}\tau}+\overline{k}_{\eta j}l_j y_{cj-1}(\tau)\\
&+(-\beta\overline{k}_{fj}+\beta\overline{k}_{bj}-\overline{k}_{\eta j}+\overline{k}_{\eta j+1})l_j y_{cj}(\tau)-\overline{k}_{\eta j+1}l_j y_{cj+1}(\tau)-\delta_{j1}\chi\mu(1-f_n)l_1 u^2\alpha_1(\tau)\\
&+(-\overline{k}_{\alpha j}+\overline{k}_{\eta j}l_{j-1}l_j)\alpha_{j-1}(\tau)+\{(\beta^2\overline{k}_{fj}+\beta^2\overline{k}_{bj}+\overline{k}_{\eta j}+\overline{k}_{\eta j+1})l_j^2+\overline{k}_{\alpha j}+\overline{k}_{\alpha j+1}-2\chi\mu l_j u^2\}\alpha_j(\tau)\\
&+(-\overline{k}_{\alpha j+1}+\overline{k}_{\eta j+1}l_j l_{j+1})\alpha_{j+1}(\tau)+\delta_{jN}\mu\left\{\chi(1-f_t)-\frac{2C_b}{\pi}\right\}l_N u^2\alpha_N(\tau)=0,\quad \text{for } j=1 \text{ to } N.
\end{aligned}\tag{17}$$

The linearized dimensionless equations of motion are rewritten in matrix form

$$[M]\left\{\begin{matrix}\ddot{y}\\ \ddot{\alpha}\end{matrix}\right\}+[C]\left\{\begin{matrix}\dot{y}\\ \dot{\alpha}\end{matrix}\right\}+[K]\left\{\begin{matrix}y\\ \alpha\end{matrix}\right\}=\{0\},\tag{18}$$

where $[M]$ is the mass, $[C]$ the damping, and $[K]$ the stiffness matrix; $\{y|\alpha\}^{\mathrm{T}}=\{y_1,\alpha_1,y_2,\alpha_2,\ldots,y_N,\alpha_N\}^{\mathrm{T}}$ is the vector of the generalized coordinates. Solutions are then sought of the form

$$\left\{\begin{matrix}y\\ \alpha\end{matrix}\right\}=\left\{\begin{matrix}\overline{y}\\ \overline{\alpha}\end{matrix}\right\}\exp(\mathrm{i}\omega t)=\left\{\begin{matrix}\overline{y}\\ \overline{\alpha}\end{matrix}\right\}\exp(\lambda t);\tag{19}$$

substituting into the previous equation we obtain

$$(\lambda[I]-[Y])\{\overline{\phi_j}\}=\{0\},\tag{20}$$

in which $\lambda=\mathrm{i}\omega$; non-trivial solutions are obtained for $\det(\lambda[I]-[Y])=0$, yielding $2N$ eigenvalues of the matrix $[Y]$, λ_j. The generally complex eigenvalues λ_j of the system permit the assessment of (linear) stability for each set of system parameters. For a stable system, the λ_j are either real and negative or complex conjugate pairs with negative real parts. The corresponding eigenvectors are $\{\overline{\phi_j}\}$.

Critical values of any given system parameter, in our case the flow velocity u, are associated with the state of neutral stability of the system, where the eigenvalues of the linearized system contain a purely imaginary pair or a single zero value. When the critical values are surpassed, the system becomes unstable.

2.7. LTB and LEB trains

Here we give the definition of LTB and LEB trains. First, we give the relationship for stiffness of the discrete and continuous systems of the LTB system. The moment and shear forces acting on an element of the continuous model are given by

$$M = \frac{EI}{\rho_r}, \quad Q = k'AG\phi,$$

where ρ_r is the radius of curvature, A the cross-sectional area, E Young's modulus, I the second moment of the cross-sectional area, and $k'G$ the effective shear modulus. Those of the discrete model are

$$M = k_\alpha \alpha, \quad Q = k_\eta l_c^* \phi,$$

where l_c^* ($=2l^*$) is the length of each car. By letting the moment and shear forces of the continuous system be equal to those of the discrete one, we obtain

$$k_\alpha = \frac{EI}{\rho_r \alpha} = \frac{EI}{l_c^*}, \quad k_\eta = \frac{k'AG}{l_c^*}. \tag{21}$$

The rotational and translational spring constants, k_α and k_η, interconnecting the cars are related to the flexural and shear rigidity of the continuous system via Eq. (21). Based on these relationships, the discrete system of the train of cars may be converted into a continuous Timoshenko-beam system and hence the present model of the train of cars can be considered as a lumped-parameter Timoshenko-beam (LTB) model [19]. A significant feature of this system of flexibly interconnected cars is that, unlike a Timoshenko beam in which the flexural and shear rigidities are interrelated in terms of the material properties, in this case flexural and shear rigidities are related to different sets of springs; hence, by altering the values of these springs, the equivalent Timoshenko model can be made to approach the Euler–Bernoulli model (instead of doing so by slenderness considerations). Next, in order to obtain the equivalent continuous Euler–Bernoulli beam system, the Timoshenko beam effects of rotational inertia and shear deformation will be neglected. Neglecting rotational inertia implies that the mass-moment of inertia is zero ($J \to 0$). To neglect the shear deformation effect, the translational springs interconnecting the cars are given very large values (i.e. $k_\eta \to \infty$, or say, 10^{15}), so that the cars cannot undergo lateral translational motion. In fact, letting $J \to 0$ and $k_\eta \to \infty$ (i.e. $G \to \infty$, see Eq. (21)) in the Timoshenko equation [31],

$$EI\frac{\partial^4 y}{\partial x^4} + m\frac{\partial^2 y}{\partial t^2} - \left(J + \frac{EIm}{kAG}\right)\frac{\partial^4 y}{\partial x^2 \partial t^2} + \frac{Jm}{kAG}\frac{\partial^4 y}{\partial t^4} = p(x,t) + \frac{J}{kAG}\frac{\partial^2 p}{\partial t^2} - \frac{EI}{kAG}\frac{\partial^2 p}{\partial x^2}, \tag{22}$$

we obtain the Euler–Bernoulli equation,

$$EI\frac{\partial^4 y}{\partial x^4} + m\frac{\partial^2 y}{\partial t^2} = p(x,t). \tag{23}$$

In addition, we employ the relation $k_\alpha = EI/l_c^*$ in Eq. (21). In the previous study [19], we have undertaken a comparison between the present model and the pinned–pinned continuous Euler–Bernoulli beam, because a certain amount of work for pinned–pinned continuous systems had been studied in the past. The values of the variables of the present model are chosen in order to reduce the model to the equivalent continuous Euler–Bernoulli beam model. It has been shown that the present model is in good agreement with previous results for pinned–pinned continuous systems, which further verifies the methodology of the present model. In addition, the present lumped-parameter Timoshenko-beam (LTB) model can replicate the dynamical behaviour of a continuous Euler–Bernoulli beam under certain conditions [19]. Also, because it was shown that the overall dynamical behaviour of the *lumped-parameter* Euler–Bernoulli (LEB) model and that of the *continuous* Euler–Bernoulli model subjected to fluid dynamic forces are similar to each other [26], the LTB model can replicate the dynamical behaviour of the LEB model [19].

3. Local and distributed imperfections of disordered LTB and LEB trains

Table 1 presents the system parameters employed in this study. The number of cylinders of the LEB and LTB trains is set at $N=16$, which is a typical number of cars in high-speed trains in Japan. All dampers (dashpots) of the system are set to zero to highlight the effects of disorder.

Local and *distributed* imperfections are taken into account by independently changing the mass constants, m (and mass-moment of inertia, J_c), and the spring stiffnesses, k (k_f, k_b, k_α, or k_η), of the system shown in Fig. 1. *Local* imperfections involve a different component substructure property (mass m, and the spring stiffnesses k_f and k_b) in a single car in the middle (or end) of the other, identical ones. *Distributed* imperfections involve a deviation in the mass, m, and the supporting spring stiffnesses, k_f and k_b, and the components of the coupler, the rotational stiffness, k_α, and the translational

Table 1
Values of system parameters for a finite-length train in a tunnel.

$N=16$	$2l_j$ ($=l_{car}$)=14.1 (25 m)	L_A=226.0 (400 m)
a=1.77 m	$\beta=0.72$	R^*/a=2.24
A/A_d=0.2	$A'/A=0$	$\rho_f=1.23\,\mathrm{kg/m^3}$
$\rho_{car}=151.6\,\mathrm{kg/m^3}$	C_T=0.01288	$C_N=C_T/2$=0.00644
C_D=0.0	C_b=0.157	f_n=1.0
f_t=0.8	$k_f=k_b$=353 000 N/m ($=k_0$)	$k_\alpha=30\,000\,000\,\mathrm{Nm/rad}$
$k_\eta=9800\,\mathrm{N/m}$	All dampers=0	

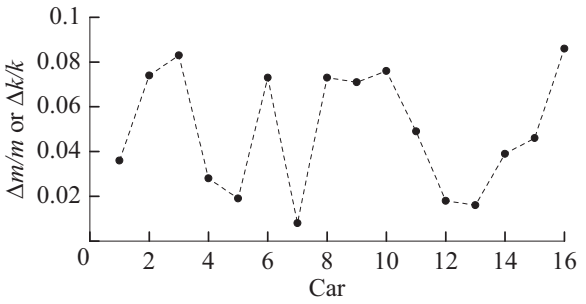

Fig. 5. Random imperfections in mass m or spring stiffness k, with uniform probability in the interval [0, 0.1].

stiffness, k_η, between cars with a distribution of random imperfections between 0 and 10 percent of the "perfect" value; thus, $\Delta m/m$ and $\Delta k/k$ are random variables with a uniform probability density function in the interval [0, 0.1], as shown in Fig. 5. The imperfections in Fig. 5 are produced by using a random number generator. (Note that results of a similar qualitative nature can be obtained if we employ other random imperfections of [0, 0.1] instead of those in Fig. 5.) For the sake of clarity, it is assumed that the stiffnesses $k_{f,j}$ and $k_{b,j}$ in the same car have the same random variables as in Fig. 5. This distributed imperfection may represent realistic operating conditions for the following reasons: (a) the car mass is different in locomotives and vehicles, and it varies with the number of passengers; and (b) springs cannot be manufactured precisely identical. Moreover, springs usually become stiffer with age due to permanent strain [32].

Note that imperfections in J_c and k_η will not be considered in the LEB model, but only in the LTB model, since in the former the effects of rotational inertia and shear deformation are ignored.

4. Mode localization in the LTB model in still fluid

Here we consider the possibility of mode localization in a lumped-parameter Timoshenko-beam (LTB) model.

4.1. Local imperfections

As explained in the previous section, local imperfections will be taken into account by independently changing the mass, m, and the spring stiffnesses, k_f and k_b, of a single car in the middle (or end) of an otherwise uniform train, where m, k_f, and k_b are the structural components of the car. Two cases of local imperfections of *disordered* supporting springs will be investigated, namely with $k_{fj=5}=k_{bj=5}=0$ and $k_{fj=16}=k_{bj=16}=0$; the results will be compared with those of the *ordered* system. Since this study deals with train-like articulated systems as well as trains, and additionally intends to show a difference of mode localization phenomena between the LTB and LEB systems, not only 10 percent random variations but also drastic local imperfections ($k_f=k_b=0$) will be considered.

The mode shapes of the lowest three modes of LTB trains with *ordered* (open circles) or *disordered* (solid circles) supporting springs in the *middle* car—$k_{fj=5}=k_{bj=5}=0$—are illustrated in Fig. 6. Note that the open or solid circles correspond to the ends of each car and the horizontal lines in-between to the car bodies. Mode 1, the fundamental mode for the *ordered* (open circles) supporting springs has no nodes, which is a typical for coupled bodies with free-free boundary conditions; mode 2 for the ordered system has a node at the centre of the train, and mode 3 has two nodes. Note that the ordered system of the Timoshenko beam seems to behave purely as a shear beam where the rigid bodies of the chain do not rotate ($\alpha=0$), although they could. This is because k_α is given a very large value of $30\times10^6\,\mathrm{N\,m/rad}$ as presented in Table 1, so that the rotational displacement of the rigid bodies of the chain is relatively small, compared to the translational one (k_η is 9800 N/m).

The mode shapes for the disordered system are different. The translational displacement of the middle car, Car 5, in mode 1 is much larger than the others, which are actually motionless; motion is trapped within Car 5, clearly indicating

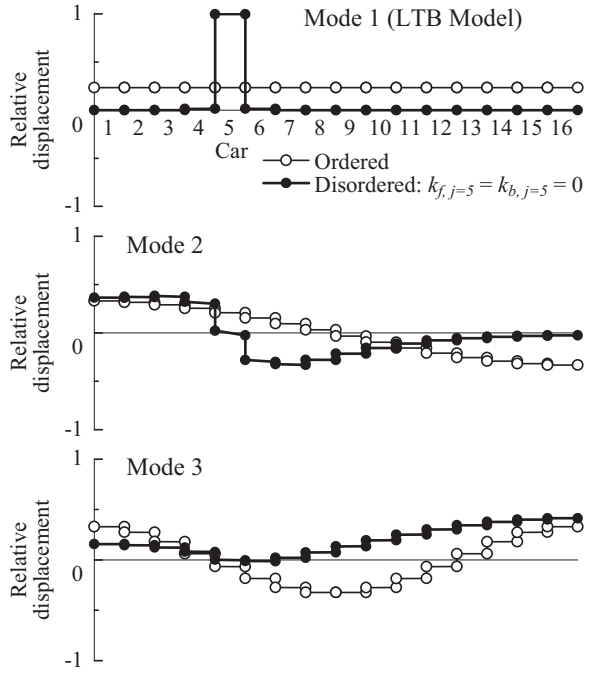

Fig. 6. Lowest three modes of LTB model with *local* imperfections in k_f and k_b: $k_{fj=5}=k_{bj=5}=0$; $u=0$.

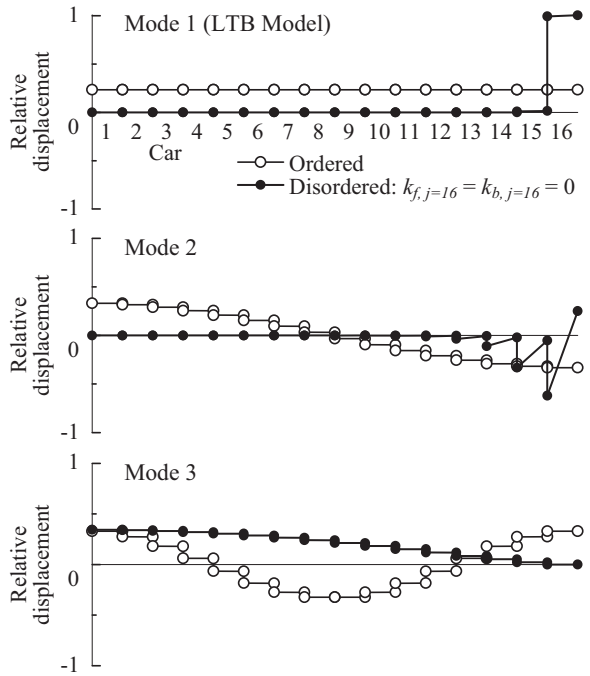

Fig. 7. Lowest three modes of LTB model with *local* imperfections in k_f and k_b: $k_{fj=16}=k_{bj=16}=0$; $u=0$.

mode localization. In contrast, in modes 2 and 3, the displacement of Car 5 is much smaller than the others and there is no mode-trapping for these modes.

Next, the mode shapes of the LTB trains with disordered supporting springs in the *tail-end* car—$k_{fj=16}=k_{bj=16}=0$—are given in Fig. 7. The translational displacement of Car 16 of mode 1 is much larger than the others, just as in the case of Car 5 in Fig. 6. In mode 2, the rotational displacements of the last few tail-end cars are much larger than the others. Conversely,

in mode 3, the displacement of Car 16 is much smaller than the others. That is, motion in modes 1 and 2 seems to be trapped within the few tail-end cars, but not in mode 3.

These results in Figs. 6 and 7 indicate that LTB models with *local* imperfections in the supporting springs result in mode localization phenomena. Next, local imperfections in the mass, m, are examined. When the mass of Car 5 is doubled, for instance, mode localization is observed, similar to that for the case of the supporting springs discussed above; hence, no figures are presented.

From all these results, we can conclude that LTB models with *local* imperfections in the mass or the supporting springs of the car components display mode localization phenomena. Note that this type of mode localization, due to *local* imperfections, is roughly predictable from the distribution of imperfections. All the mode localization phenomena discussed above are related to the specific car attached via disordered supporting springs or having an imperfection in mass.

4.2. Distributed imperfections

As mentioned in Section 3, distributed imperfections involve changing independently the mass, m, or the springs, k (k_f, k_b, k_α, or k_η), by an amount Δm or Δk, where $\Delta m/m$ or $\Delta k/k$ are random variables with uniform probability density function in the interval [0,0.1] as in Fig. 5.

The mode shapes of the disordered system with distributed imperfections in the mass, m, are shown in Fig. 8, as well as those for the ordered system. In mode 1, the translational displacement of the last few tail-end cars for the disordered system (solid circles) is much larger than the others, which are actually motionless. In mode 2, the displacements of a few leading cars are much larger than the others. Similarly, in mode 3, the displacements of a few of the middle cars are much larger than the others. From these mode shapes, it is evident that energy in modes 1, 2, and 3 is trapped within the tail-end, the leading, and the middle cars, respectively, with the others remaining almost stationary. The three modes have different locations of peak displacement which cannot be perfunctorily predicted from the distribution of imperfections in Fig. 5.

Next, the mode shapes of the train with imperfections in the supporting spring stiffnesses, $k_{f,j}$ and $k_{b,j}$, are shown in Fig. 9. As in the case of mass imperfections, the motions here in modes 1, 2, and 3 are trapped within some adjacent cars, i.e. about Car 13, Car 6, and Car 6 of the train, respectively, with the others remaining virtually motionless.

Finally, the mode shapes of the train with imperfections in the rotational, k_α, or translational, k_η, springs between cars are shown in Fig. 10. Note that the effects of k_α and k_η have been examined separately, but practically the same results are obtained, as shown in Fig. 10. The mode shapes of the disordered and ordered systems are almost coincident; i.e., the system is practically unaffected by the distributed imperfections in the rotational or translational springs between the cars; no mode localization occurs.

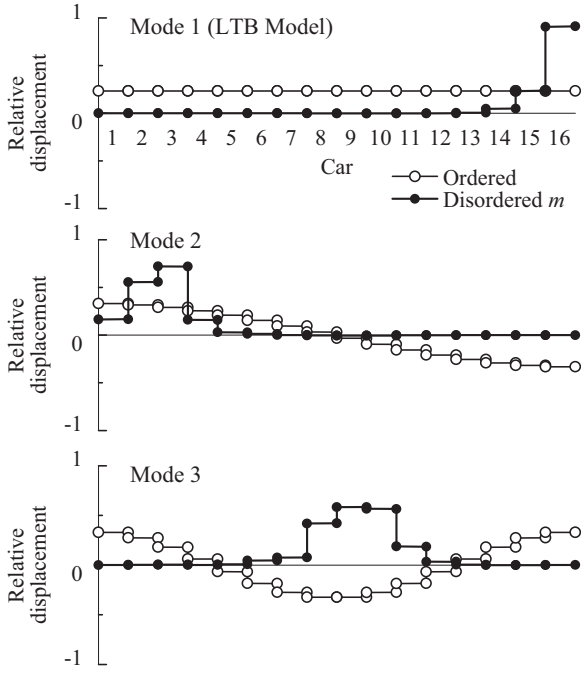

Fig. 8. Mode localization of the lowest three modes of LTB model due to *distributed* imperfections in m: 10 percent random variation in m; u=0.

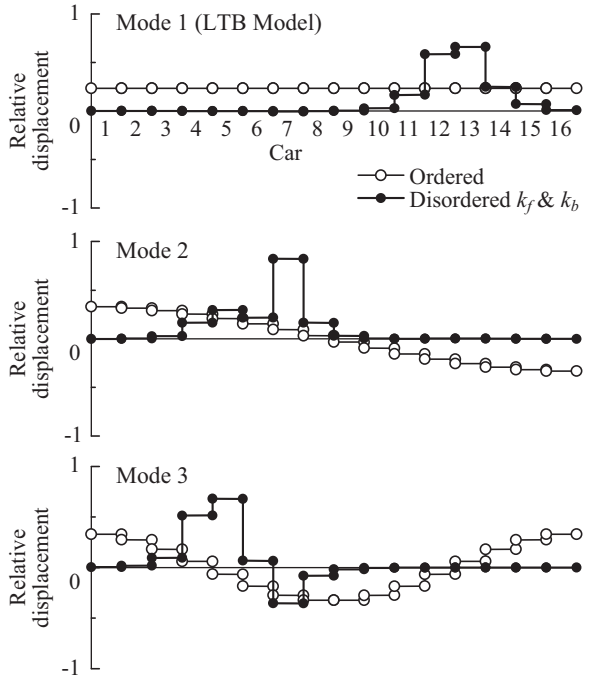

Fig. 9. Mode localization of the lowest three modes of LTB model due to *distributed* imperfections in k_f and k_b: 10 percent random variation in k_f and k_b; u=0.

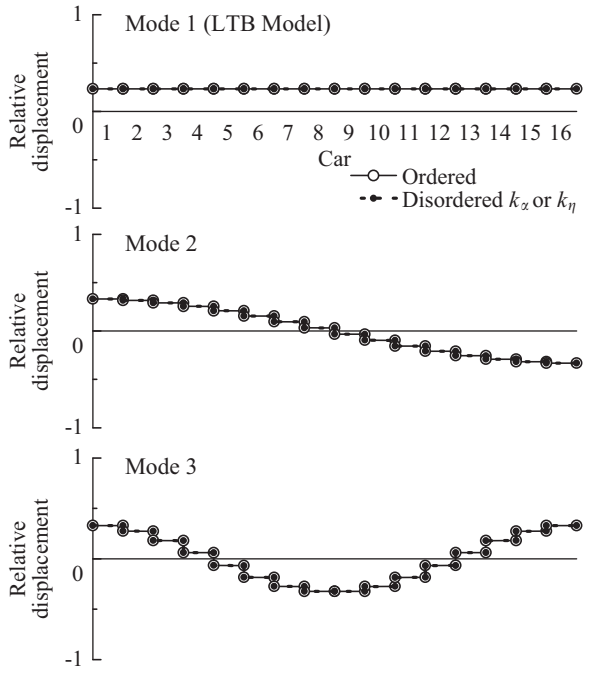

Fig. 10. No mode localization of the lowest three modes of LTB model due to *distributed* imperfections in k_α or k_η: 10 percent random variation in k_α or k_η; u=0.

From the foregoing results, it is shown that the LTB models with either local or distributed imperfections in the mass, m, and the supporting spring stiffnesses, k_f and k_b, which are the component properties of the car and thus affect the natural frequencies of the system, exhibit mode localization phenomena; in contrast, distributed imperfections in the springs k_α or k_η which couple the cars together do not give rise to any mode localization. Table 2 summarizes these results.

Table 2
Conditions of mode localization of the LTB and LEB models due to imperfections in mass and springs.

Parameter of train	Mass: m		Supporting springs: k_f, k_b		Springs between cars: k_α,k_η
Imperfections	Local	Distributed	Local	Distributed	Distributed
LTB model	**ML**	**ML**	**ML**	**ML**	No
LEB model	**ML**	No	**ML**	No	No

ML=Mode localization.

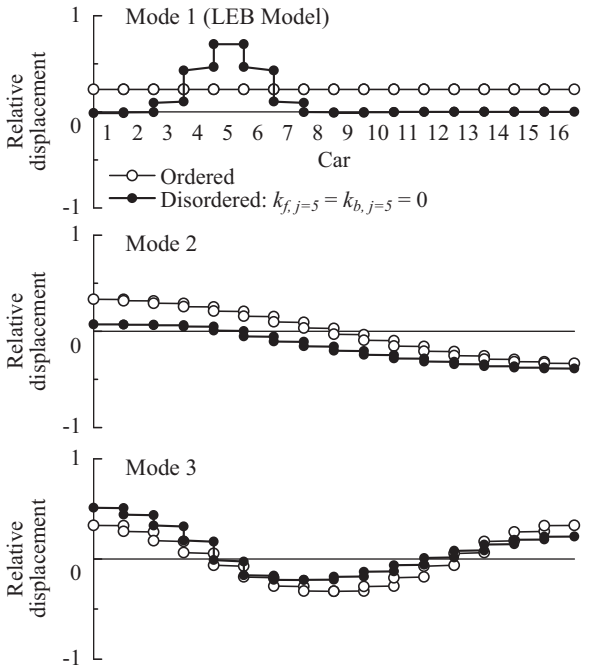

Fig. 11. Lowest three modes of LEB model with *local* imperfections in k_f and k_b: $k_{fj=5}=k_{bj=5}=0$; $u=0$.

Note that qualitatively similar results are obtained if we employ other random imperfections, say of $[0, -0.1]$ instead of $[0, 0.1]$.

5. Mode localization in the LEB model in still fluid

In the previous section, the effects of the *local* and *distributed* imperfections on mode localization phenomena of the LTB model have been studied. Here, in the same way, mode localization phenomena in the Euler–Bernoulli beam (LEB) model will be examined. Note that, in the LEB model, the effects of rotational inertia and shear deformation are ignored, as mentioned in Section 2.7.

5.1. Local imperfections

The mode shapes of the disordered system with local imperfections in the supporting springs of the middle car ($k_{fj=5}=k_{bj=5}=0$), as well as those for the ordered system, are shown in Fig. 11. (Note that the mode shapes of the *ordered* LEB model virtually coincide with those of the LTB model.) In mode 1 of the disordered system, the translational displacement of a few of the middle cars around Car 5 (solid circles) is much larger than the others which remain almost stationary. Motion in mode 1 seems to be trapped around Car 5. On the other hand, in modes 2 and 3, the displacements of Car 5 are much less than the others; moreover, there is no trapping of motions within the train. As mentioned previously in Section 2.7, the value of k_η in the LEB train is not truly infinite but very large (say, 10^{15}) and thus shear strains in the eigenmodes of LEB are observed.

In the same manner, local imperfections in the supporting springs for the tail-end car ($k_{fj=16}=k_{bj=16}=0$) and in the mass (doubling the mass), for the same car are examined separately. Mode localization phenomena are observed just as in the case of Car 5 above; hence, no figures are given here. Thus, we conclude that LEB models, with *local* imperfections in either the mass or supporting springs, demonstrate mode localization.

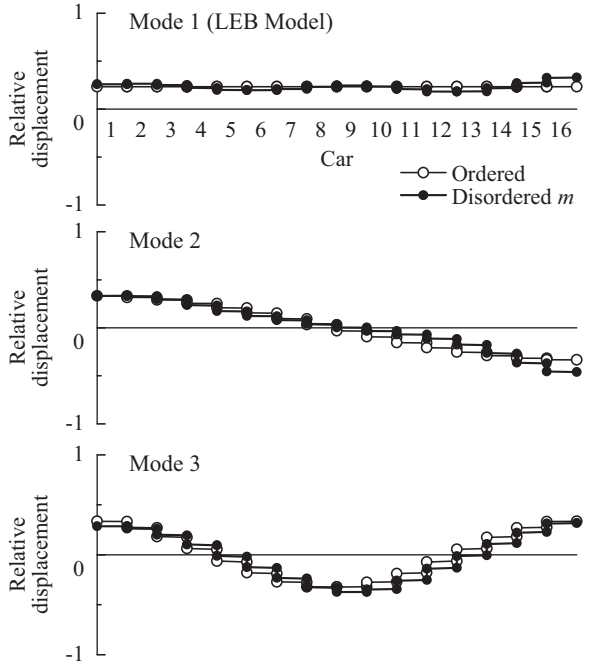

Fig. 12. No mode localization of the lowest three modes of LEB model due to *distributed* imperfections in m: 10 percent random variation in m; $u=0$.

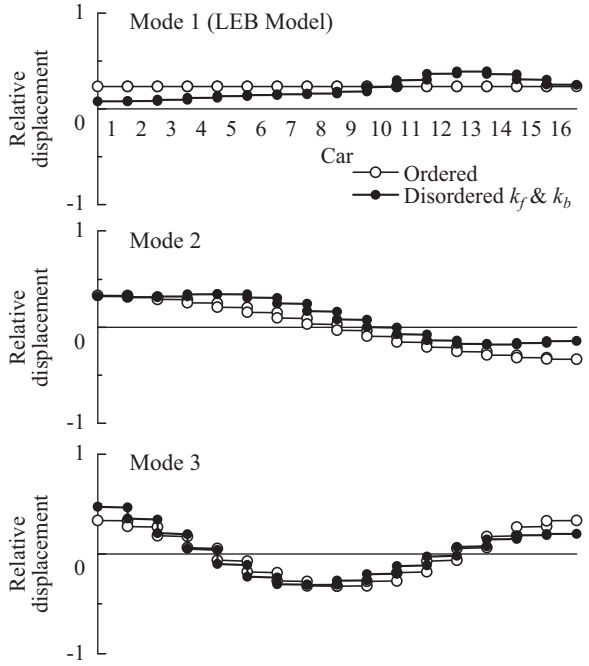

Fig. 13. No mode localization of the lowest three modes of LEB model due to *distributed* imperfections in k_f and k_b: 10 percent random variation in k_f and k_b; $u=0$.

It is remarked again that this type of mode localization due to *local* imperfections is roughly predictable from the distribution of imperfections; all the mode localization phenomena discussed above are related specifically to the cars attached to the disordered supporting springs or the cars with imperfections in mass.

5.2. Distributed imperfections

The effect of distributed imperfections in the mass, m, and the spring stiffnesses (k_f and k_b, k_α, and k_η) are investigated separately. First, the mode shapes of the disordered system with distributed imperfections in the mass, m, and the supporting springs, k_f and k_b (which are components of the cars) are shown along with the mode shapes of the ordered system in Figs. 12 and 13, respectively. The mode shapes of the disordered system (solid circles) are similar to those of the ordered one (open circles). It is seen that LEB models with *distributed* imperfections in the mass, m, or the supporting springs, k_f and k_b, exhibit no mode localization. Next, in the same way, the effects of k_α and k_η, which couple the components of the car together, on mode localization are examined independently. Again, no mode localization phenomena are observed, just as in Fig. 10. It is concluded that the LEB models with distributed imperfections do not demonstrate mode localization phenomena.

It should be mentioned that *weak* localization seems to have occurred in the LEB models with distributed imperfections in the mass (Fig. 12) and the spring stiffnesses k_f and k_b (Fig. 13) because the mode shapes of the disordered systems are similar but they are different to those of the ordered ones. Since the amplitude decay per substructure for weak localization is much smaller than that for strong localization, the effect is not significant for systems consisting of a limited number of substructures like the present system, but it is for those of several hundreds or thousands of substructures such as atom chains and lattices in Physics [12].

6. Discussion of mode localization in the LTB and LEB models in still fluid

Conditions of mode localization for the LTB and LEB models due to imperfections in mass and springs are summarized in Table 2. It is seen that mode localization phenomena are observed in all cases (both LEB and LTB models) with *local* imperfections in mass and supporting springs. On the other hand, mode localization phenomena due to distributed imperfections can be observed only in the LTB model with distributed imperfections in *mass* and *supporting* springs. That is, for the LTB train, distributed imperfections in mass and supporting springs, which are components of the car and thus affect the natural frequencies of the system, have a great influence on mode localization phenomena, while the springs between cars, which couple these components together, have less effect. On the contrary, LEB models with distributed imperfections exhibit no (strong) localization phenomena. Hence, the Timoshenko beam effects of rotational inertia and shear deformation have a great influence on mode localization phenomena. These results (in still air) are expected to be sensibly the same as for the system in vacuum.

When the LEB model is considered, the members of the chain are strongly coupled, so that localization can occur only for very large (local) imperfections. If, in contrast, almost the same degree of imperfections is distributed along the chain, the distributed local defects are not sufficient to trigger *strong* localization but *weak* localization, which has little effect on the dynamics of most engineering structures and is thus of little interest here. Note that these conclusions are in good agreement with previous results that show that structures with strong coupling between substructures are not expected to display (strong) localization phenomena, e.g. Refs. [11,12], and that Timoshenko beam effects have a great influence on mode localization [15].

It was shown in Ref. [19] that the dynamics (stability) of LEB and LTB theories are fundamentally different in the conditions for positive work to be done by the fluid on the system for the clamped-free LEB and free-free LTB models. This essential difference between the LEB and LTB systems may explain the reason why the LTB train is more susceptible to mode localization than the LEB train.

It should be noted that the location of peak displacements for mode localization due to *distributed* imperfections may be more difficult to predict than those due to *local* ones, because the location of the localization is related to the cars associated with the disordered components, while for distributed imperfections this is not true.

7. Dynamics of the disordered LTB model subjected to flow

In the foregoing sections, mode localization phenomena in the LTB and LEB models *in still fluid* ($u=0$) have been investigated by examining mode shapes. In this section, the dynamics of the disordered systems of LTB trains *subjected to flow* will be investigated. As in previous sections, two kinds of disordered systems will be studied: (i) with local imperfections, specifically with $k_{fj=16}=k_{bj=16}=0$; and (ii) with distributed imperfections in the supporting springs—the distribution of random imperfections of [0, 0.1] in k_f and k_b. First, for reference, the mode shapes of the *ordered* LTB train system subjected to flow will be compared with those in still fluid. Then, a stability analysis is undertaken, yielding Argand diagrams showing the real and imaginary parts of the eigenvalues of the ordered and disordered systems as a function of the dimensionless flow velocity u. In addition, mode shapes of the disordered system subjected to flow will be illustrated and compared with those in still fluid.

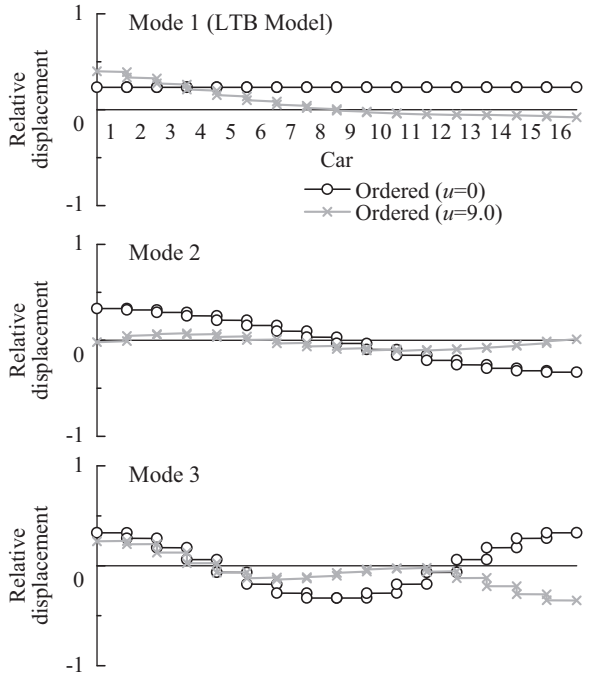

Fig. 14. Mode shapes for the lowest three modes of the lumped-parameter Timoshenko-beam (LTB) train with no imperfection, subjected to flow.

7.1. Mode shapes of the ordered system

Fig. 14 shows the mode shapes of the modes with the lowest three frequencies for the LTB train, with and without flow (u=0 and 9.0). (The reason for choosing u=9.0 will be explained in the next subsection.) The mode shapes of the system subjected to flow (x symbol) are different from those in still fluid (open circles), thus illustrating that the fluid dynamic forces acting on the system modify the mode shapes [19,25]. The extent of these changes in mode shapes will be noted for estimating the effect of the fluid dynamic forces on the disordered systems.

7.2. Local imperfections

The stability of the disordered system with *local* imperfections in the supporting springs—$k_{f,j=16}=k_{b,j=16}=0$—is investigated first. Fig. 15 gives the Argand diagram of the lowest three eigenvalues of an LTB train, with ordered and disordered supporting springs. The upper figure is an enlarged view of the upper part of the Argand diagram close to $\mathrm{Im}(\lambda)\simeq 0.37$.

First, the dynamical behaviour of the *ordered* system (hollow symbols) is discussed. As seen in the upper figure, with increasing flow velocity, starting from zero, free oscillations of all three modes are damped. As the flow velocity increases further, however, the damping in mode 1 is diminished and the system may become unstable by dynamic instability at a value of u slightly higher than $u\simeq 9.0$, where the locus eventually crosses the $\mathrm{Im}(\lambda)$−axis. However, $\mathrm{Re}(\lambda)$ for modes 2 and 3 is always negative, and thus the system remains always stable in these modes. This is a typical dynamical behaviour of the lumped-parameter Timoshenko-beam (LTB) train with ordered supporting springs, cf. Ref. [19].

Next, the dynamical behaviour of the *disordered* system (solid symbols) with $k_{f,j=16}=k_{b,j=16}=0$ is discussed. Free oscillations in all three modes are damped for relatively small u, as before. As the flow velocity is increased further, however, the system may become unstable by flutter in mode 3 at $u\simeq 8.3$; i.e., the instability is associated with a different mode number and flow velocity than for the ordered system. In the same way, at $u\simeq 10.0$, the system may become unstable by flutter in mode 2. On the other hand, in mode 1 at $u\simeq 10.961$, the frequencies become purely real, bifurcating on the $\mathrm{Re}(\lambda)$−axis; the first branch of this mode goes through the origin ($\mathrm{Re}(\lambda)>0$) at $u\simeq 10.982$, indicating buckling.

These results indicate that, even though only the tail-end car is "defective" ($k_{f,j=16}=k_{b,j=16}=0$), that is, only one-sixteenth of the supporting springs in the train are deleted, the dynamical behaviour of the LTB ordered train system changes considerably in the following ways: (a) the ordered system may become unstable by flutter only in mode 1, while the disordered system loses stability by flutter first in mode 3 and then in mode 2, and finally by bucking in mode 1; (b) the critical flow velocity is reduced from $u\simeq 9.0$ in mode 1 to $u\simeq 8.3$ in mode 3; and (c) the frequencies of oscillation of the system, which are proportional to the imaginary parts of the eigenvalues, are significantly different.

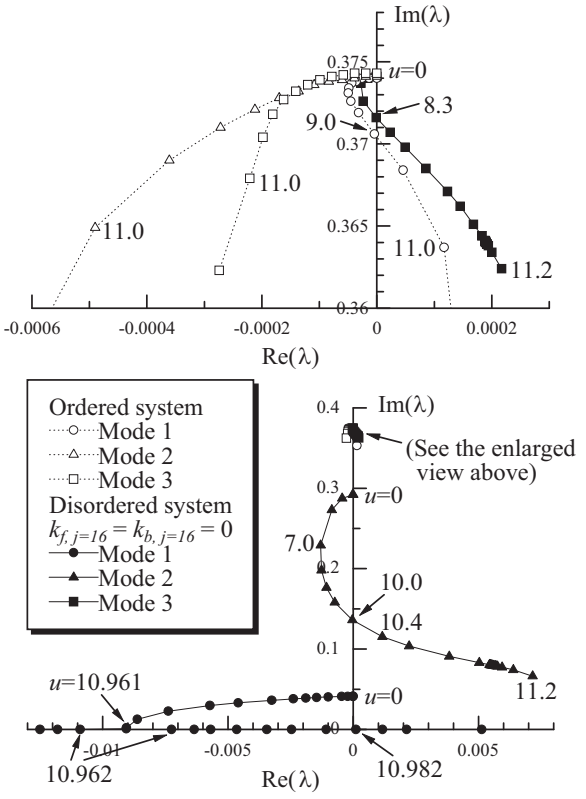

Fig. 15. Argand diagram of the lowest three eigenvalues of the lumped-parameter Timoshenko-beam (LTB) train with ordered and disordered supporting springs ($k_{fj=16}=k_{bj=16}=0$). The upper figure is the enlarged view of the part of Im(λ)−axis about 0.37 in the lower figure.

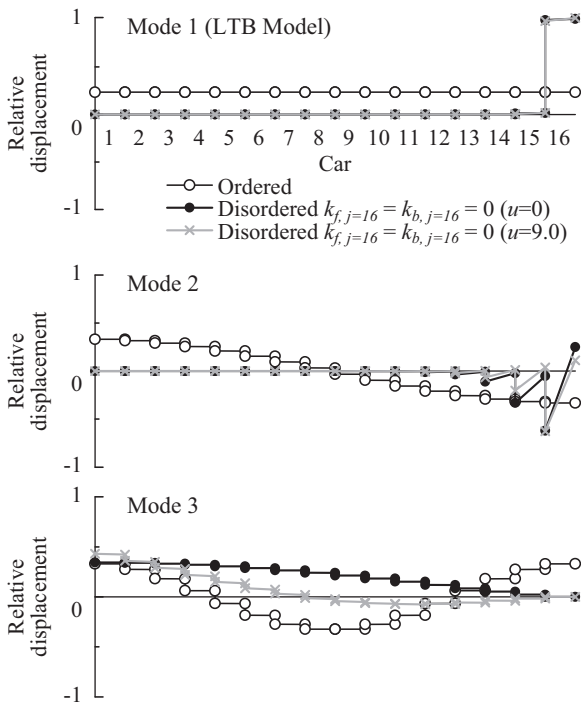

Fig. 16. Mode shapes of the lowest three modes of the lumped-parameter Timoshenko-beam (LTB) train with disordered supporting springs subjected to flow : $k_{fj=16}=k_{bj=16}=0$.

Finally, the mode shapes of the disordered system at $u=0$ and 9.0, together with the ordered one at $u=0$ are shown in Fig. 16. It is now clear why we have selected the flow velocity of $u=9.0$: the ordered system becomes unstable by flutter at $u \simeq 9.0$ as shown in Fig. 15. It is apparent that the mode shapes of the disordered system both at $u=0$ and 9.0 (solid and x symbols) are significantly different from those of the ordered ones shown in Fig. 14.

7.3. Distributed imperfections

The stability of the disordered system with *distributed* imperfections in the supporting springs—the distribution of random imperfections of [0, 0.1] in k_f and k_b—is investigated. Fig. 17 gives the Argand diagram of the lowest three eigenvalues of the LTB train with ordered and disordered supporting springs. The dynamical behaviour of the ordered and disordered systems can be discussed in the same manner as in Section 7.2. The results in Fig. 17 indicate that increasing the supporting spring stiffnesses randomly up to 10 percent may change the dynamical behaviour of the LTB train in the following ways: (a) the order in which modes go unstable is changed, i.e., at first, the ordered system may become unstable by flutter in mode 1, while the disordered system loses stability by flutter in mode 2, mode 3 and then in mode 1; and (b) the critical flow velocity is increased from $u \simeq 9.0$ in mode 1 to $u \simeq 9.3$ in mode 2.

Finally, the mode shapes of the disordered system at $u=0$ and 9.0, together with the mode shapes of the ordered system at $u=0$ are shown in Fig. 18. It is seen that the mode shapes with disordered imperfections both at $u=0$ and 9.0 (solid and x symbols) are significantly different from those of the ordered ones shown in Fig. 14.

8. Conclusions

With the aid of a simplified model for a high-speed train moving in a tunnel, mode localization and stability of disordered trains of flexibly interconnected *rigid bodies* with elastic supports subjected to fluid dynamic forces are investigated numerically by examining mode shapes and eigenvalues. The conditions of mode localization in the LEB and LTB trains due to imperfections in the mass and the springs have been clarified.

The main findings obtained from this study are summarized as follows:

(i) Rotational inertia and shear deformation effects, taken into account in the LTB model, have a considerable influence on mode localization phenomena.

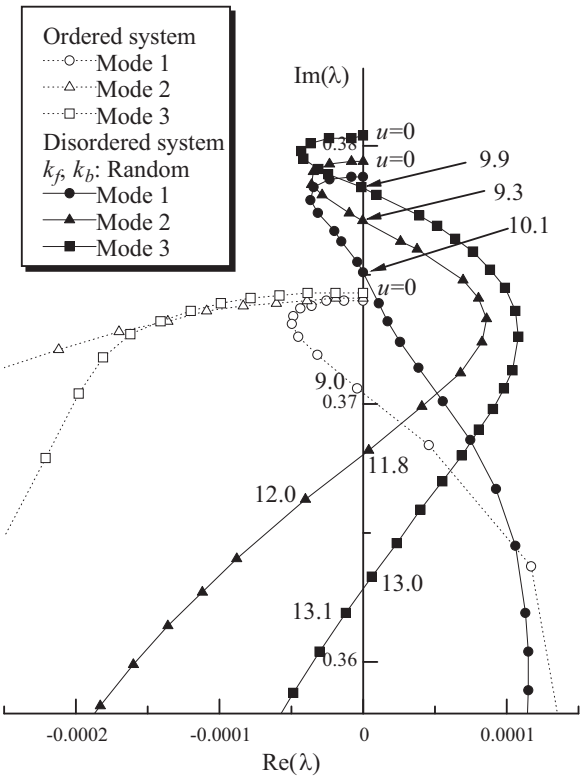

Fig. 17. Argand diagram of the lowest three eigenvalues of the lumped-parameter Timoshenko-beam (LTB) train on ordered and disordered supporting springs: *distributed* imperfections in k_f and k_b.

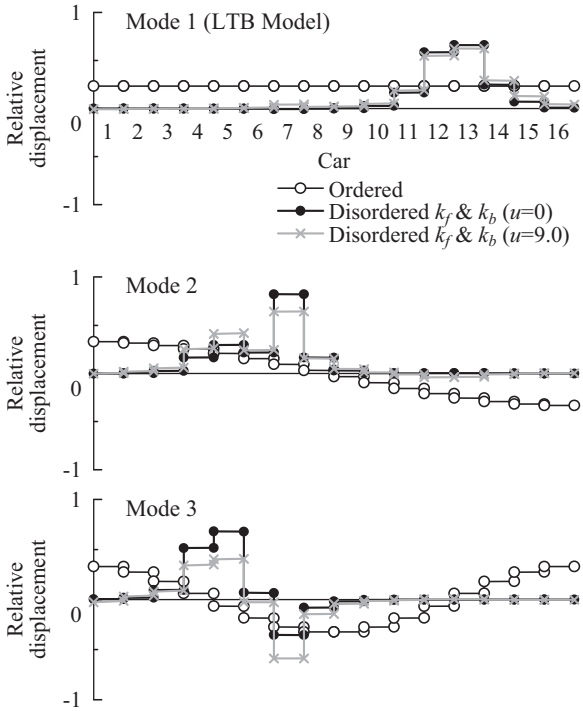

Fig. 18. Mode shapes of the lowest three modes of the lumped-parameter Timoshenko-beam (LTB) train with disordered supporting springs subjected to flow: *distributed* imperfections in k_f and k_b.

(ii) The LEB models with local imperfections in either the mass or supporting springs demonstrate (strong) localization while those with distributed imperfections do not demonstrate strong but rather weak localization.
(iii) Mode localization in the LTB model with imperfections occurs also in the presence of flow. The fluid dynamic forces acting on the system can modify the shapes of mode localization.
(iv) Imperfections in the supporting springs have a considerable influence on the stability of the LTB train. If the supporting springs on the tail-end car are removed, the LTB train may lose stability, first by flutter and then by buckling with increasing flow velocity, whereas the ordered train loses stability only by flutter.

Acknowledgment

The authors gratefully acknowledge the support by the Railway Technical Research Institute, Tokyo, Japan and the Natural Sciences and Engineering Research Council of Canada.

References

[1] T. Ishihara, M. Utsunomiya, M. Okumura, Y. Sakuma, T. Shimomura, An investigation of lateral vibration caused by aerodynamic continuous force on high-speed train running within tunnels, *Proceedings of the World Congress on Railway Research* '97, Florence, Italy, 1997, pp. 531–538.
[2] Y. Sakuma, M. Suzuki, T. Maeda, Measurement of flow around a high-speed train, *Proceedings of Fourth KSME-JSME Fluids Engineering Conference*, Pusan, Korea, 1998, pp. 177–180.
[3] M. Suzuki, A. Ido, Y. Sakuma, H. Kajiyama, Full-scale measurement and numerical simulation of flow around high-speed train in tunnel, *Journal of Mechanical Systems for Transportation and Logistics* 1 (3) (2008) 281–292.
[4] M. Suzuki, Unsteady aerodynamic force acting on high speed trains in tunnel, *Quarterly Report of RTRI* 42 (2) (2001) 89–93.
[5] M. Suzuki, K. Nakade, H. Fujimoto, Study on interaction between vehicle dynamics and aerodynamic force on high-speed train in tunnel, *RTRI Report* 15 (5) (2001) 19–24 (in Japanese).
[6] M. Suzuki, H. Fujimoto, Y. Sakuma, Measures to reduce aerodynamic force acting on high-speed train in tunnel, *Proceedings of the 11th Transportation and Logistics Conference* (*TRANSLOG 2002*), Kawasaki, Japan, 2002, JSME, Tokyo, pp. 277–278 (in Japanese).
[7] Y. Sakuma, M. Suzuki, A. Ido, H. Kajiyama, Measurement of air velocity and pressure distributions around high-speed trains on board and on the ground, *Journal of Mechanical Systems for Transportation and Logistics* 3 (1, Special issue on STECH'09) (2010) 110–118.
[8] Y. Sakuma, M.P. Païdoussis, S.J. Price, Dynamics of trains and train-like articulated systems travelling in confined fluid. Part 2: wave propagation and flow-excited vibration, *Journal of Fluids and Structures* 24 (2008) 954–976.
[9] P.W. Anderson, Absence of diffusion in certain random lattices, *Physical Review* 109 (1958) 1492–1505.
[10] C.H. Hodges, Confinement of vibration by structure irregularity, *Journal of Sound and Vibration* 82 (3) (1982) 411–424.

[11] O.O. Bendiksen, Mode localization phenomena in large space structures, *AIAA Journal* 25 (9) (1987) 1241–1248.
[12] C. Pierre, Weak and strong vibration localization in disordered structures: a statistical investigation, *Journal of Sound and Vibration* 139 (1) (1990) 111–132.
[13] A. Luongo, Mode localization in dynamics and buckling of linear imperfect continuous structures, *Nonlinear Dynamics* 25 (2001) 133–156.
[14] C. Pierre, D.M. Tang, E.H. Dowell, Localized vibration of disordered multispan beams: theory and experiment, *AIAA Journal* 25 (9) (1987) 1249–1257.
[15] S.D. Lust, P. Friedmann, O.O. Bendiksen, Localization in multi-span beams, *Proceedings of the 31st AIAA Dynamics Specialist Conference*, AIAA paper 90-1214, 1990.
[16] A. Vakakis, M.E. King, A.J. Pearlstein, Forced localization in a periodic chain of nonlinear oscillators, *International Journal of Non-Linear Mechanics* 29 (3) (1994) 429–447.
[17] A.A. Zevin, Localization of periodic oscillators in discrete non-linear systems, *Journal of Sound and Vibration* 193 (4) (1996) 847–862.
[18] G. Kerschen, M. Peeters, J. Golinval, A. Vakakis, Nonlinear normal modes, part I: a useful framework for the structural dynamicist, *Mechanical Systems and Signal Processing* 23 (1) (2009) 170–194.
[19] Y. Sakuma, M.P. Païdoussis, S.J. Price, Dynamics of trains and train-like articulated systems travelling in confined fluid. Part 1: modelling and basic dynamics, *Journal of Fluids and Structures* 24 (2008) 932–953.
[20] M. Miyamoto (Ed.), Dynamics of Railway Vehicles, JSME, 1994 (in Japanese).
[21] A. Yamamoto, Pressure variations, aerodynamic drag of train, and natural ventilation in Shinkansen type tunnel, *Quarterly Report of RTRI* 15 (4) (1974) 207–214.
[22] J.A. Schetz, Aerodynamics of high speed trains, *Annual Review of Fluid Mechanics* 33 (2001) 371–414.
[23] M.S. Howe, M. Iida, T. Maeda, Y. Sakuma, Rapid calculation of the compression wave generated by a train entering a tunnel with a vented hood, *Journal of Sound and Vibration* 297 (2006) 267–292.
[24] M.P. Païdoussis, Dynamics of cylindrical structures subjected to axial flow, *Journal of Sound and Vibration* 29 (1973) 365–385.
[25] M.P. Païdoussis, *Fluid–Structure Interactions: Slender Structures and Axial flow*, Vol. 2, Elsevier Academic Press, London, 2004.
[26] M.P. Païdoussis, Stability of a chain of cylinders travelling underwater, in: *Proceedings of the Fifth International Offshore Mechanics and Arctic Engineering Symposium, Tokyo, Japan*, ASME, New York, 1986, pp. 483–490.
[27] M.P. Païdoussis, The dynamics of clusters of flexible cylinders in axial flow: theory and experiments, *Journal of Sound and Vibration* 65 (1979) 391–417.
[28] M.J. Lighthill, Note on the swimming of slender fish, *Journal of Fluid Mechanics* 9 (1960) 305–317.
[29] G.I. Taylor, Analysis of the swimming of long and narrow animals, *Proceedings of the Royal Society (London) A* 214 (1952) 158–183.
[30] M.P. Païdoussis, Dynamics of flexible slender cylinders in axial flow. Part 1: theory, *Journal of Fluid Mechanics* 26 (1966) 717–736.
[31] W.T. Thomson, *Theory of Vibration with Applications*, fourth ed., Prentice-Hall, Englewood Cliffs, 1993.
[32] T. Azechi, M. Suzuki, M. Hansaka, Evaluation of durability of air spring for railway vehicles, *RTRI Report* 15 (3) (2001) 47–52 (in Japanese).